Strål
säkerhets
myndigheten
Swedish Radiation Safety Authority

Author: Magnus Dahlberg,
Dave Hannes,
Thomas Svensson

Research

2015:38

Evaluation of fatigue in austenitic stainless steel pipe components

Report number: 2015:38 **ISSN:** 2000-0456
Available at www.stralsakerhetsmyndigheten.se

SSM perspective

Background

Transferability of experimental results obtained for smooth test specimens under constant amplitude loading to realistic components subjected to variable amplitude loading is an important issue in the design against fatigue. There is a lack of experimental fatigue data for austenitic steel components and the present study is an important contribution to fill this gap.

Objective

The present study is aimed to investigate the margins of the ASME design curve for austenitic stainless steel, by performing fatigue experiments on a realistic welded austenitic stainless steel piping component. A particular focus is on high cycle fatigue and variable amplitude loading.

Results

Tests at both low cycle fatigue and high cycle fatigue up to a run-out limit of 5 106 cycles were performed, and both constant amplitude and three different load spectra were applied. The main results from the study are:

- The results indicate extensive conservatism in the ASME fatigue procedure. The ASME fatigue design procedure represents a survival probability in excess of the prescribed survival probability of 95 %.
- A more detailed evaluation of the extent of the margins will largely depend on the weld fatigue reduction factor for the specific component.
- The constant amplitude results indicated longer lives in comparison to the variable amplitude results.
- The derivation of reliable design curves should be based on realistic variable amplitude loading.

The work has increased the understanding of the ASME margins and has improved the knowledge on fatigue in austenitic stainless steel components and the fundamental issue of transferability.

Need for further research

The complex material behavior of austenitic stainless steel should be further investigated in order to better describe the strains at the weld toe or strain concentration. A more precise evaluation of the strain concentration can be performed with a finite element analysis using a non-linear material model. Validation of the obtained estimate of the weld fatigue reduction factor can be performed with experimental fatigue testing of unwelded piping components.

The selection of the most appropriate fatigue model is possible with additional fatigue testing. In the current investigation this differentiation was hampered due to the limited run-out limit and large scatter in the two-level block spectrum results. The use of an increased number of test specimens would allow more detailed investigation of the observed scatter.

Project information
Contact person SSM: Björn Brickstad
Reference: SSM2012-4006

Strål
säkerhets
myndigheten
Swedish Radiation Safety Authority

Author: Magnus Dahlberg [1], Dave Hannes [1], Thomas Svensson [2]
[1] Inspecta Technology AB, Stockholm, Sweden.
[2] SP Technical Research Institute of Sweden, Borås, Sweden.

2015:38

Evaluation of fatigue in austenitic stainless steel pipe components

Date: September 2015
Report number: 2015:38 **ISSN:** 2000-0456
Available at www.stralsakerhetsmyndigheten.se

This report concerns a study which has been conducted for the Swedish Radiation Safety Authority, SSM. The conclusions and viewpoints presented in the report are those of the author/authors and do not necessarily coincide with those of the SSM.

SSM 2015:38

Table of content

1 Conclusive Summary

The current study presents an experimental investigation based on fatigue experiments of welded austenitic stainless steel pipe components, with a purpose to investigate the margins of the ASME fatigue procedure for austenitic stainless steel. The ASME design curve is obtained based on experiments with smooth test specimens and adjustment by means of corrections factors, which intend to account for transferability.

The presented work partially made up for the shortcoming of experimental data on realistic austenitic stainless steel components, with particular focus on high cycle fatigue and variable amplitude loading. Both constant amplitude and three different load spectra were applied during the different fatigue tests. The main findings of the current investigation are:

- The results indicate extensive conservatism in the ASME fatigue procedure.
- The ASME fatigue design procedure represents a survival probability in excess of the prescribed survival probability of 95 %.
- A more detailed evaluation of the extent of the margins will largely depend on the weld fatigue reduction factor for the specific component.
- Further research is required to improve the accuracy and control of the estimated fatigue limit.
- Fatigue testing of a realistic component allows more realistic margins and component specific design curves, consequently improving the control of potential fatigue risks linked to the considered component.
- The derivation of reliable design curves should be based on realistic variable amplitude loading.
- The determination of variable amplitude strength could be standardized to a standard spectrum type without much loss of generality.
- The constant amplitude results indicated longer lives in comparison to the variable amplitude results.
- The complex non-linear behavior of austenitic stainless steel was highlighted.

The work has increased the understanding of the ASME margins and has improved the knowledge on fatigue in austenitic stainless steel components and the fundamental issue of transferability.

Further investigation of the issue is however recommended so as to further elaborate and validate the findings of the present study.

2 Nomenclature

a	Factor in DFL model
A	Factor in Langer equation
b	Exponent in DFL model
B	Exponent in Langer equation
c	Initial fatigue limit in DFL model
C	Asymptotic fatigue limit in Langer equation
C_2	Secondary stress index defined in ASME [1]
E	Young's modulus
i	Dummy index
k_M	Slope of moment- nominal strain diagram
K	Fatigue reduction factor
K_2	Local stress index defined in ASME [1]
m	Total number of strain cycles in a load sequence
M	Applied moment
n	Total number of strain cycles in a load sequence with amplitudes exceeding the fatigue limit
N	Total number of cycles, predicted or experimental fatigue life
N_c	Total number of load cycles with strain amplitudes exceeding the fatigue limit in DFL model
N_C	Total number of load cycles with strain amplitudes exceeding the constant fatigue limit C
R_m	Tensile strength
$R_{p0.2}$	Yield strength
α	Factor in Basquin equation
β	Exponent in Basquin equation
ε	Strain
ε_0	Mean nominal strain (due to internal pressure)
ε_a	Strain amplitude
ε_Y	Yield strain
σ	Standard deviation of error of predicted logarithmic life
$\hat{\blacksquare}$	Estimated quantity
$\blacksquare_{max}$	Maximum value

3 Introduction

3.1 Background

The ASME Boiler and Pressure Vessel Code specifies rules for construction of nuclear facility components in section III [1]. Design curves and specific methods for fatigue analysis are included for various types of materials such as austenitic steels type 304/316. A design curve is typically obtained after correction of a mean curve, which represents a 'best fit' with experimental data from large databases. These databases contain results of fatigue experiments generally performed in laboratories on small, smooth test specimens in air. The correction factors applied to the mean curve intend to deal with the fundamental problem of transferability to real components. The uncertainties in the predicted fatigue life of real components are related to environmental, material and loading effects, which were often not considered in the experimental data at the base of the derived mean curve.

Transferability is a difficult problem with large uncertainties, but essential in understanding and preventing fatigue in real or relevant components. Transferability is, amongst others, affected by data scatter, mean stress/strain, surface finish, size, welding, environment, loading conditions, etc. [2] In the ASME Boiler and Pressure Vessel Code [1] the adjustment of the mean curves is performed with correction factors on the strain (or stress) or the cycles, whichever is more conservative. The correction factor on number of cycles has mainly an effect for low-cycle fatigue (LCF), i.e. for less than 10^4 cycles. An additional correction for low amplitudes consists of a Goodman correction to account for the effects of tensile mean strain (or stress) [3]. This correction especially affects the design curve in the high cycle fatigue (HCF) regime. Component testing or fatigue experiments under more realistic conditions including different environmental, material or loading effects allow to validate the margins in the ASME design curves and quantify the degree of conservatism.

3.2 Austenitic stainless steel

Austenitic SSs are challenging materials due to the non-linear material behavior even for small strain amplitudes resulting in long lives. Relative important inelastic deformations are observed when subjected to loads in the vicinity of the constant amplitude fatigue limit [4]. At variable amplitude (VA) loading the material behavior becomes history dependent. Furthermore do austenitic SSs exhibit secondary cyclic hardening, which is likely to influence the fatigue limit. Experimental fatigue investigations generally use strain as fatigue governing parameter. The classic S-N or Wöhler curves are then obtained by multiplying the strain amplitude with Young's modulus. The resulting stress amplitude does therefore not correspond to the actual stress in the specimen, when inelastic material behavior occurs.

In the current version of the ASME Boiler and Pressure Vessel Code [1] the design curve for austenitic SS is based on the adjustment of the mean curve derived by ANL [2]. The available fatigue experiment databases for austenitic SS, used in the determination of the mean curve, include mainly strain controlled fatigue tests performed on small, smooth test specimens in air, whereas little experimental data is available for austenitic SS components. The adjustment of the ANL mean curve was performed using a factor of 2 on the strain (or stress) and 12 on the cycles, see Figure 1. The correction factor on the cycles was previously, prior to 2010, equal to 20, which based on a statistical study [2] yielded too large conservatism. This modification has however mainly an impact for LCF. A final correction to obtain the tabulated ASME design curve consists of a Goodman type correction to account for effects of tensile mean strain.

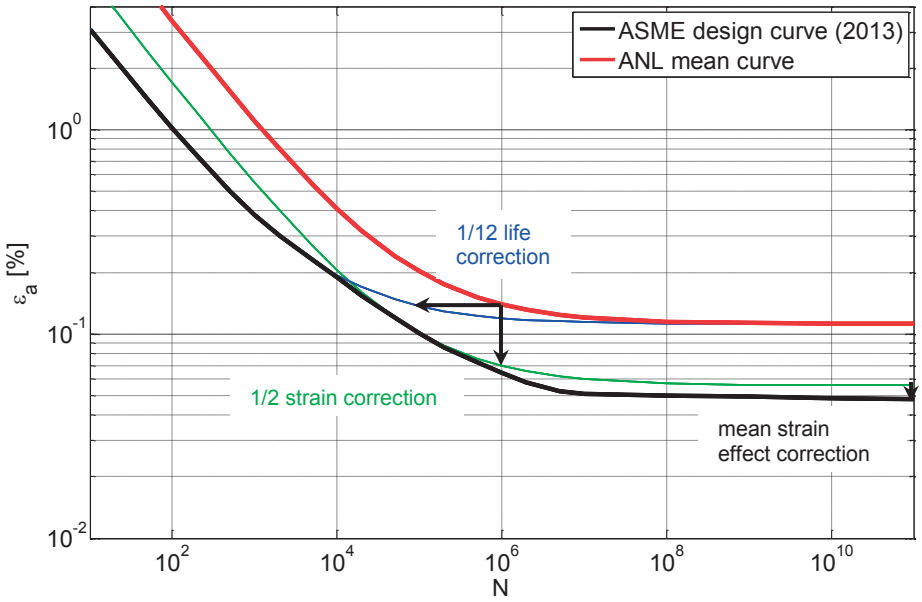

Figure 1. Derivation of the ASME design curve based on the ANL mean curve. The curves are intended for use in conjunction with the local strain amplitude.

Experimental studies with displacement control on austenitic SS type 304 components were performed by Heald and Kiss [5] using straight pipes and elbows, Lu [6] and Cheng [7] investigated welded austenitic SS type 304 components. These studies focused on LCF component testing with constant amplitude (CA) loading. At CA testing the test specimen is subjected to a load oscillating between a constant minimum and maximum value until failure occurs. Fatigue failure with tests on smooth specimens is generally determined by a pre-defined reduction of the peak or steady-state stress, whereas for component testing leakage typically defines fatigue failure.

The data used for the mean curve for austenitic SS mainly deal with LCF. The lack of data for VA fatigue testing at HCF on austenitic SS components was high-lightened in the literature study by Dahlberg and Bremberg [3]. Such testing conditions correspond to more realistic loading scenarios of real-life components in nuclear power plant (NPP) piping systems, and allow in particular the study of the margins in the ASME design curve for SS at HCF.

3.3 Objectives

The current study aims at making up for the shortcoming of experimental data on realistic austenitic SS components, with particular focus on HCF and variable amplitude loading. The experimental study allows increased understanding of the margins in ASME, especially for HCF, which previous component testing at LCF could not provide. The effect of this shortcoming on the mean curve and the correction factors for austenitic SS required closer investigation.

The study aims also at improving knowledge on the fundamental issue of transferability. Given the complex material behavior of austenitic SS, component testing may be necessary to provide more precise fatigue life predictions. The use of different VA spectra during testing of the piping components allowed the investigation of potential effects on fatigue life. A final purpose with the current study was the improved understanding of fatigue in austenitic SS and in particular in the investigated real component, allowing the improvement of the control of potential fatigue risks related to the studied piping component.

4 Experimental Study

The results in the current investigation were obtained with a limited number of test specimens and realistic testing conditions. A new fixture for performing the experiments was developed.

4.1 Test specimens

A total of 30 test specimens were manufactured from 60 straight, seamless TP 304 LE stainless steel pipes produced in two batches: lot 21192 and 54306. An illustration of the chemical composition and tensile properties at room temperature are presented in Table 1 and 2, respectively. The pipe outer diameter was 60.33 mm with a wall thickness equal to 5.54 mm. The pipes were partially machined to introduce shoulders by reducing the outer diameter until a remaining wall thickness of approximately 3 mm. At the edge of each pipe a single v-edge was prepared. Figure 2 presents the geometry of the test specimens prior to the welding process in more detail. Concentricity of the pipes was verified to avoid unwanted results.

Table 1. Chemical composition as percentage by weight [weight%] for each lot.

Lot	C	Si	Mn	P	S	Cr	Ni	Mo
21192	0.011	0.36	1.14	0.016	0.005	18.18	10.07	0.11
54306	0.010	0.39	1.13	0.023	0.006	18.32	10.14	0.09
	W	Co	Ti	Cu	Nb	Ta	B	N
21192	0.01	0.022	<0.005	0.053	<0.01	<0.005	<0.0004	0.058
54306	0.01	0.026	<0.005	0.043	0.01	<0.005	<0.0004	0.055

Table 2. Average tensile properties at room temperature for each lot.

Lot	Yield strength $R_{p0.2}$ [MPa]	Tensile strength R_m [MPa]	Elongation [%]	Young's modulus E [GPa] (*)	Poisson's ratio [-]
21192	288	617	53	200	0.3
54306	274	614	51		

(*) Sandvik 3R12.

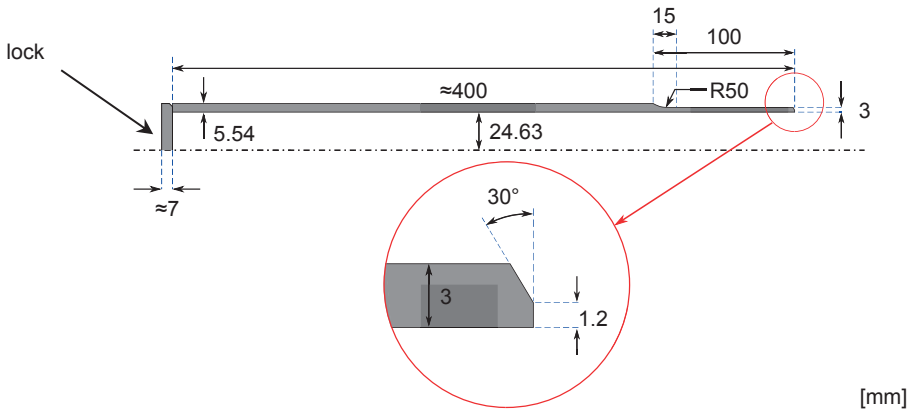

Figure 2. Schematic of the geometry of the piping components prior to welding.

Pipes from the same batch were then joined with a circumferential single v-joint butt weld and tested in as-welded condition, see Figure 3. Additionally, the pipes were fitted with approximately 7 mm thick butt welded locks to allow pressurizing during the experiments. The locks were equipped with a hole to allow control of the internal pressure, see Figure 3(a). The realistic welded piping components were manufactured in compliance with nuclear requirements.

Radiographic examination of the weld joints according to EN 1435 B was performed to identify faulty welds. Lack of fusion and pores were revealed in the welding joint for pipe 12. A pore was also discovered in the weld of piping component 17. The remaining piping components complied with acceptance level 1 specified in EN 12517-1. Test specimen 12 was used during pre-testing and set-up of the experimental procedure, thus preserving the remaining specimens for the actual experimental study. Pipe 17 was subjected to CA fatigue testing resulting in early fatigue failure, presumably due to the defective welding joint. The results for both pipe 12 and 17 were not included in the current experimental fatigue investigation. A total of 28 test specimens were however available for the fatigue experiments.

(a) Close-up views of the performed butt welds on a finished test specimen.

(b) Different test specimens after welding and prior to undergoing fatigue testing.

Figure 3. Final state of the welded piping components.

4.2 Experimental set-up

4.2.1 Equipment and instrumentation

The experimental set-up consisted of an inventive construction allowing for reversed bending loading with displacement control in a standard single axis servo-hydraulic testing machine, see Figure 4. Bending testing was selected to get a constant nominal load over a larger length of the straight test specimen, i.e. between the fixtures or shoulders, where the weld joint was situated. A conventional 4-point bending test set-up was considered to be unsuitable for fatigue testing at relatively high frequencies. A bending moment was therefore generated by means of custom-built fixtures, acting as torque arms. The fixtures were mounted at less than 10 mm from the shoulders of the test specimens.

The used experimental set-up, see Figure 4, does however not induce a pure bending state between the fixtures. The alternating bending stress is in fact superposed by an alternating membrane stress due to the presence of an axial force. For the investigated piping component and the proposed experimental set-up, the membrane stress was less than 5% from the maximum bending stress for linear elastic material behavior, which was considered to be negligible. A longer torque arm would effectively reduce the relative contribution of the membrane stress, but the need for increased displacement amplitudes would then result in the adverse effect of reduced maximum test frequency.

During the design of the experimental set-up special care was taken to minimize and to some extent prevent difficulties such as wear at connections, mechanical play and complex stress distributions. The experimental set-up allowed for flexible and convenient testing. The design of the piping components and test equipment ensured that the fatigue process was governed by the local weld conditions, which is also the case for real components.

Furthermore, a conventional strain gage was mounted on the test specimen at approximately 50 mm from the weld joint, to avoid any influence of the conditions in the vicinity of the weld joint. The strain gage was situated in the bending plane, which allowed capturing the nominal bending strain. During the pre-testing phase of the experimental series four strain gages were used, whose results indicated that one strain gage was sufficient for the actual fatigue experiments, regardless the loss of redundancy in case of a failing strain gage. Furthermore the recorded nominal strain was found to be linearly related to the applied displacement, which supported the use of displacement control in the performed fatigue experiments. The proportionality factor was estimated to be approximately 25.3 mm/%. This factor tended however to decrease somewhat during the fatigue experiments, due to non-linearity. This effect was especially observed for tests involving large strain amplitudes, but was nevertheless assumed of relative little effect on the actual applied nominal strain amplitudes, on which the fatigue analysis was based.

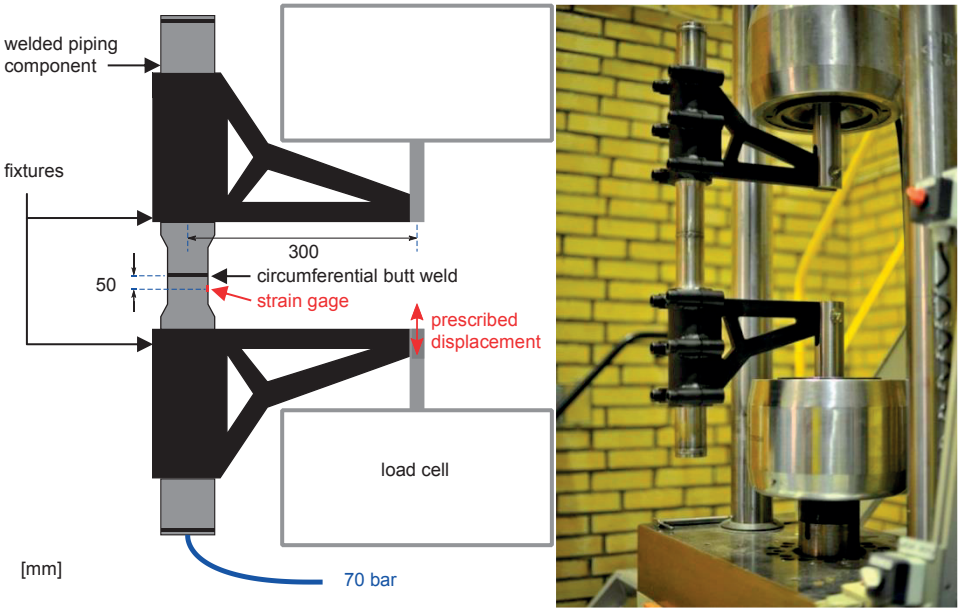

Figure 4. Schematic of custom-built experimental set-up for alternating bending fatigue testing, including illustration of actual mounted test specimen in servo-hydraulic testing machine.

4.2.2 Testing procedure

The fatigue experiments were displacement controlled with load ratio approximately equal to minus unity. Hence the minimum and maximum strains have approximately same magnitude but with opposite signs. Displacement control closely resembles thermal expansion and anchor movement loads present in piping systems, allowing for fatigue testing with variable amplitude load spectra relevant for nuclear piping. During the course of the fatigue experiments the resulting force in the load cell and the nominal strain in the test specimen were recorded continuously with sampling frequency 200 Hz. The tests were performed in air at room temperature (RT), avoiding environmental effects on the fatigue behavior of the piping component, which was out of the scope of the current investigation. The presence of corrosive environments which could accelerate fatigue failure is namely also not accounted for in the ASME fatigue design curves, see NB-3121 in [1].

The piping components were furthermore water pressurized allowing for a realistic failure criterion based on leakage, i.e. the experiments were stopped when a pre-set constant internal pressure could no longer be sustained. Alternatively fatigue experiments were stopped when a run-out limit of 5 million cycles was reached or exceeded.

4.3 Load description

The 28 piping components included in the experimental test series were subjected to four different load types, which were scaled to different severities. Both constant amplitude and variable amplitude tests were performed, see summary in Table 3.

Each component was also pressurized during testing, which in combination with the bending load introduced a multi-axial load state, relevant to real piping components. The constant internal pressure was 70 bar and yielded a small constant tensile mean strain in the axial direction of approximately $\varepsilon_0 = 0.0054$ %, based on linear elastic material behavior. This mean strain was considered small

compared to the applied maximum strain amplitudes. Increased test frequencies are convenient to reduce the total testing time. The testing frequency in the accelerated fatigue experiments was nevertheless limited to avoid too large strain rates. No strain rate effects on the fatigue behavior were expected during the fatigue experiments at RT, as these effects tend to appear for higher temperatures [2]. In the current investigations strain rates did usually not exceed 6%/s. An exception were the experiments with VAP, where maximum strain rates could reach about 10%/s.

Table 3. Summary of different load types considered in the fatigue experiments.

Load type		Total number of tests	Number of tested severities
Constant amplitude (CA)		10	6
Variable amplitude (VA)	Piping spectrum (VAP)	7	4
	Gaussian spectrum (VAG)	6	3
	Two-level block spectrum (VA2)	5	1

4.3.1 Constant amplitude (CA)

The 10 constant amplitude experiments were performed with sinusoidal prescribed displacement signals with frequencies in the range 6 – 10 Hz. The severity of the prescribed displacement was determined by its amplitude: 1.7, 1.8, 1.95, 2.2, 2.6 and 2.8 mm. The corresponding strain amplitudes were in the range 0.06-0.12%.

4.3.2 Variable amplitude (VA)

Variable amplitude was imposed by use of three different load spectra. The test frequency for the variable amplitude experiments depended on the severity. Slightly increased test frequencies were used for experiments with lower strain amplitudes. The variable amplitude loads were applied in blocks of about 400-450 cycles. Any block load effects were assumed to be small, especially for the HCF tests.

4.3.2.1 Piping spectrum (VAP)

The spectrum based on characteristic piping loads (VAP) was constructed from expected pressure vessel loads. The obtained spectrum was close to regular, i.e. with irregularity factor equal to unity, which means that all load cycles cross the mean value of the load. From the obtained level-crossing spectrum and the irregularity factor, a mathematical description of the spectrum was constructed [8]. An appropriate time signal was computed based on sinusoidal transitions between consecutive maximum and minimum values. The amplitude and frequency of the time signal could then be adjusted to get an appropriate input signal for the testing machine. Figure 5 illustrates the obtained time signal for the piping spectrum. A normalized level crossing diagram for the piping spectrum is shown in Figure 6. It was computed from the time signal in Figure 5(b).

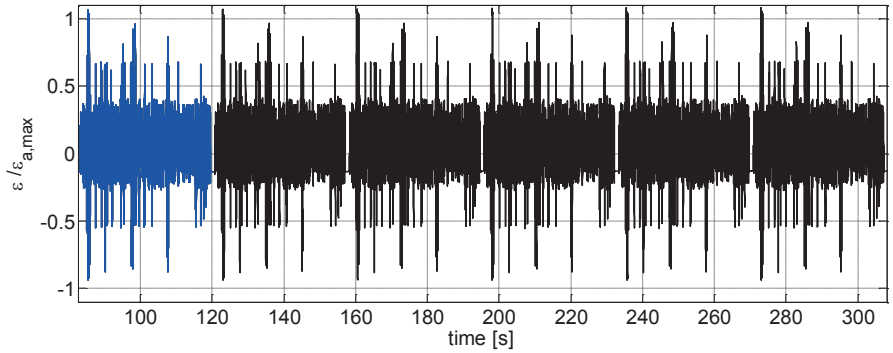

(a) A sequence of 6 load blocks.

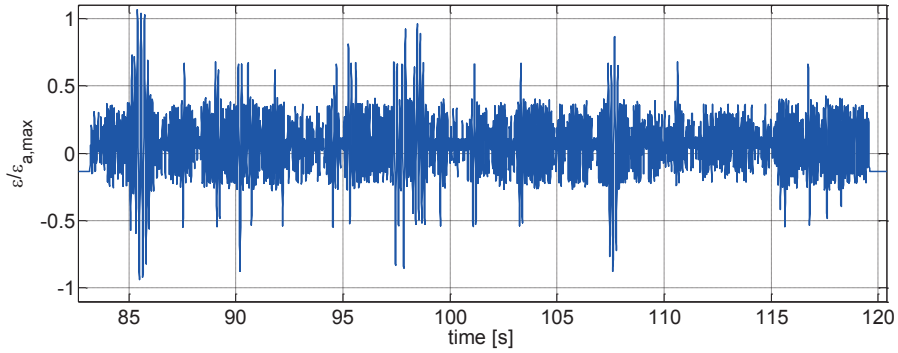

(b) Close-up view of one VAP load block containing 437 load cycles.

Figure 5. Piping spectrum (VAP) constructed from characteristic piping loads. Normalized nominal strain vs time.

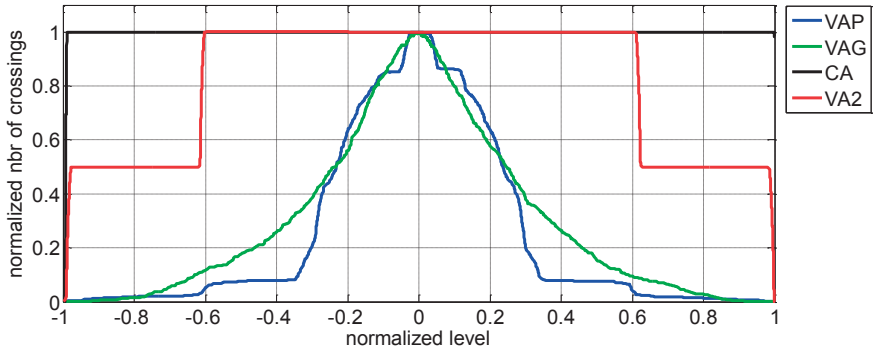

Figure 6. Normalized level crossing diagrams for the different load types. The zero normalized level corresponds to the mean nominal strain level.

Four severities were investigated, denoted as low, medium, high and peak severity. The corresponding maximum strain amplitudes were in the range 0.12 – 0.29%. All nominal strain amplitudes remained below the yield strain only for the low load severity, whereas the maximum nominal strain amplitude for the peak severity corresponded approximately to twice the yield strain. The piping spectrum does however only include a relatively small number of cycles with large strain amplitudes, as shown by the shallow tails in the level crossing diagram in Figure 6. The frequencies of the load spectrum ranged between 6-12 Hz, with a dominant frequency of about 7.5Hz.

4.3.2.2 Gaussian spectrum (VAP)

A Gaussian spectrum was constructed based on the piping spectrum. Its properties are illustrated in Figures 6 and 7. The cycles with large amplitudes are more frequent in the Gaussian spectrum compared to the piping spectrum, as illustrated by the thicker tails in the level crossing diagram in Figure 6. The normalized level crossing diagram for the Gaussian spectrum was computed form the block signal in Figure 7(b).

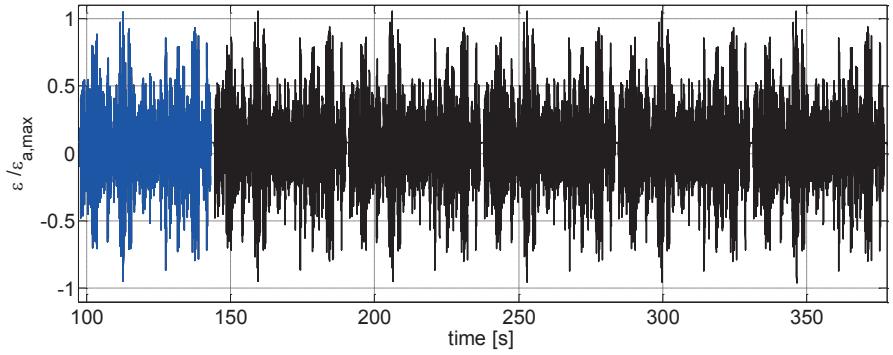

(a) A sequence of 6 load blocks.

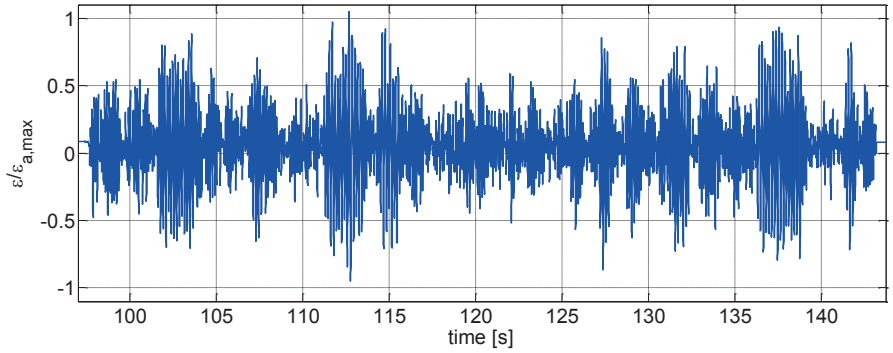

(b) Close-up view of one VAG load block containing 427 load cycles.

Figure 7. Gaussian spectrum (VAG). Normalized nominal strain vs time.

The prescribed displacement signal based on the Gaussian spectrum has a dominant frequency of 6.3 Hz. Three severity levels were examined by scaling up the magnitude of the prescribed displacement. Two fatigue tests were performed for each severity level. The medium severity level yielded maximum strain amplitude slightly below the yield strain of 0.141%. The high and low severity levels had maximum strain amplitudes of about ±30% of the maximum strain amplitude for the intermediate level.

4.3.2.3 Two-level block spectrum (VA2)

The constructed two-level block spectrum (VA2) contained a load sequence consisting of two strain amplitude levels at 0.069 and 0.042% with equal number of cycles, see Figures 6 and 8. Each block consisted of a sub-block at the high level followed by a sub-block at the low level. The prescribed displacement signal was sinusoidal with frequencies 10 and 12.5 Hz for respectively the high and low level. The VA2 spectrum was constructed to investigate the studied fatigue life models. Due to the prescribed strain amplitudes, the VA2 spectrum consisted of only one severity level. A total of 5 fatigue tests were performed using this load spectrum. This spectrum was designed to discriminate between the studied fatigue life models.

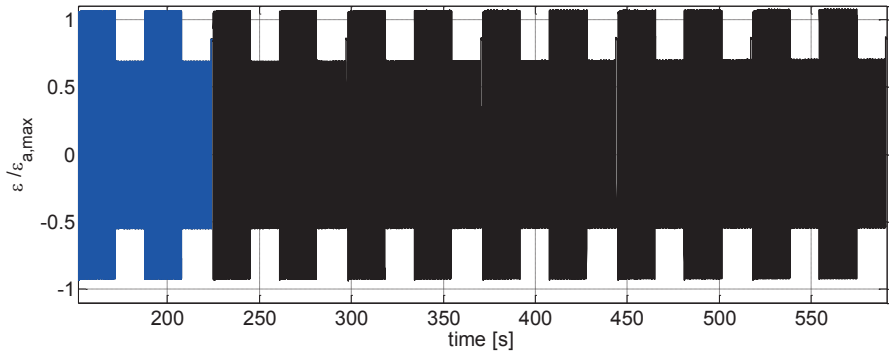

(a) A sequence of 6 load blocks, consisting each of two elementary VA2 blocks.

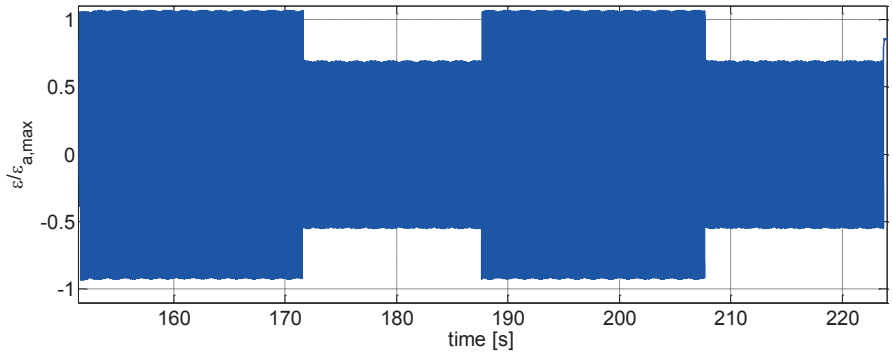

(b) Close-up view of one load sequence consisting of two VA2 load blocks containing each 400 strain cycles.

Figure 8. Two-level block spectrum (VA2).

5 Theory and Methods

5.1 Fatigue life models

Different models exist to predict the number of cycles to component failure as function of a load parameter, such as stress or strain amplitude. In the current experimental investigation the selected fatigue governing parameter was the measured strain amplitude, which allowed direct comparison with ASME predictions and the study of the ASME margins. It should be noted that the use of the strain amplitude as fatigue governing parameter was shown to be inaccurate when considering fatigue [3]. More appropriate fatigue governing parameters should include both stress and strain, as for instance the SWT parameter [9], allowing for a better correlation, but would not allow for the study of the ASME margins. Furthermore is a relevant stress measure difficult to compute, considering the complex material behavior displayed by austenitic SS, especially at high cycle fatigue (HCF).

The experimental results from the performed alternating fatigue bending tests on welded piping components were investigated with three different models with a scalar strain amplitude load parameter. The original models were generalized to be applicable with variable amplitude loading. A norm or equivalent strain amplitude was therefore introduced based on Palmgren-Miner's linear damage rule [10,11]. This hypothesis is in accordance with the ASME procedure. The methodology of this procedure is further developed in [12]. The three different models differ by the way they include the fatigue limit, i.e. the limit below which no fatigue damage is expected to occur.

5.1.1 Basquin model

Basquin's equation without a fatigue limit is a classic approach to model high cycle low strain amplitude fatigue.

5.1.1.1 Constant strain amplitude

A linear relation in logarithmic form is assumed, between the strain amplitude ε_a to the total number of load cycles, N [13].

$$N = \alpha \, \epsilon_a^{-\beta} \tag{1}$$

The constants α and β are typically determined by comparison to experimental data from constant amplitude testing. The exponent β is directly related to the slope of the curve in a logarithmic plot.

5.1.1.2 Variable strain amplitude

For variable amplitude loading, the strain amplitude in Equation (1) is replaced by an equivalent strain amplitude $\| \varepsilon_a \|_\beta$, which gives the same accumulated damage as the full spectrum.

$$N = \alpha \left(\| \epsilon_a \|_\beta \right)^{-\beta} \tag{2}$$

The equivalent measure for a load sequence consisting of m strain cycles with amplitude $\varepsilon_{a,i}$, is expressed in terms of the β-norm of the strain amplitudes.

$$\|\epsilon_a\|_\beta = \left(\frac{1}{m} \sum_i^m \epsilon_{a,i}^\beta \right)^{1/\beta} \quad (3)$$

The identification of the load cycles and different strain amplitude levels included in the load spectrum can be performed by classic rain flow counting algorithms. Note that all strain amplitude levels contribute in the equivalent strain amplitude in the Basquin relation. The presence of a fatigue limit below which strain amplitudes do not cause damage, is not accounted for.

5.1.2 Langer model

The Langer model [14] uses a modified expression of the Basquin relation in Equation (1) including a cut-off limit representing the effect of a constant fatigue limit. It introduces a characteristic curved shape for long lives. The design curves in the ASME standard [1] are based the results presented by [2] using the Langer model.

5.1.2.1 Constant strain amplitude

The Langer equation is expressed in terms of A and B, analogues to constants α and β in Equation (1), and constant C representing a constant fatigue limit and introducing an asymptote in the model.

$$N = A\,(\epsilon_a - C)^{-B} \quad (4)$$

The expression is only valid for a strain amplitude larger than C. Lower strain amplitudes are assumed not to contribute to the fatigue damage. This model was used for the ANL mean curve in Figure 1, with A=983.4, B=1.92, and C= 0.112 % [2].

5.1.2.2 Variable strain amplitude

For variable amplitude loading, the strain amplitude in Equation (4) is replaced by a new equivalent strain amplitude $\| \varepsilon_a \|_{BC}$, which gives the same accumulated damage as the full spectrum.

$$N = A\,(\,\|\epsilon_a\|_{BC} - C\,)^{-B} \quad (5)$$

The equivalent BC-norm of the strain amplitude is expressed by analogy with Equation (3), in terms of constants B and C.

$$\|\epsilon_a\|_{BC} = \left(\frac{1}{n} \sum_i^n \left(\epsilon_{a,i} - C\right)^B \right)^{1/B} + C \quad (6)$$

The sum only includes the n cycles for which $\varepsilon_{a,i} > C$, i.e. the cycles causing fatigue damage according to the Langer model. Furthermore the sum is also normalized by

n. A load spectrum will cause fatigue damage for $\| \varepsilon_a \|_{BC} > C$, otherwise the number of load cycles to failure is assumed to be infinite, i.e. no load cycles caused any fatigue damage.

An alternative definition of the *BC*-norm strain would be to normalize the sum with *m,* the total number of cycles actually included in the load sequence. This alternative definition would only differ from the current one proposed in Eq. (6) for load spectra including both strain amplitudes above and below the fatigue limit *C*. This alternative equivalent strain measure might be less relevant for an engineering application, but does not yield non-monotonic behavior when scaling a load spectrum including a large amount of strain cycles with small amplitudes, such as the VAP spectrum.

5.1.3 Model with decreasing fatigue limit (DFL)

The Langer model assumed the existence of a constant fatigue limit. In the current fatigue life model presented in [15], the fatigue limit is no longer a constant but decreases with time. It is namely suggested that the fatigue limit decreases as fatigue damage accumulates due to a decreasing fatigue threshold. The three parameters in the model are the Basquin parameters *a* and *b*, and an initial fatigue limit *c*.

5.2 Determination of margins

The fitting of SN curves to the experimental data allows comparing along the whole load range and not only in single points. From available experimental data, the different model parameters for each of the three selected fatigue life models are estimated by fitting using a numerical iterative scheme. The parameter estimation was based on an established probabilistic method called the maximum-likelihood method. The curves obtained from the experimental results are then compared to a reduced ASME design curve, so as to evaluate the margins.

5.2.1 Maximum-likelihood methodology

The maximum-likelihood methodology is a general method for fitting model parameters to empirical models. It is a probabilistic approach that as inputs needs,

i. a model formulation with parameters to be fit,
ii. a number of empirical observations of a property,
iii. an assumption of a random distribution type for the observed property.

In case of the three fatigue models the observed property is fatigue life and the three model formulations, Basquin, Langer and DFL have two, three and three fitting parameters, respectively. In the current investigation the model parameters were estimated using only the experimental data from the VAP and VAG load spectra, i.e. 13 observations are used for the fit.

For each model, it is assumed that the logarithm of life follows a normal distribution with the expected value according to the model and an unknown standard deviation. For an arbitrary choice of parameter values (including the standard deviation) one can then calculate a number that is proportional to the probability for the occurrence of each observation. In case of failures, this number is the normal probability density function for the observed logarithmic life, in case of a run-out, this number is the survival function for the logarithm of the tested

number of cycles, i.e. one minus the cumulative normal distribution function. The probability for the whole data set is equal to the product of the individual probabilities and proportional to the product of the calculated numbers described above, denoted the likelihood, see also [12] for more details.

The maximum likelihood estimate is then found by choosing the set of parameter values that maximizes this product. In practice this is done numerically on the logarithm of the likelihood. In case of no survivors and a linear relationship (the Basquin in log scale) this procedure is equivalent to the ordinary least squares estimate found by linear regression, which however is unable to include survivors in a consistent way. Also, the maximum-likelihood estimate can be completed with approximate confidence and prediction limits for all parameters as well as for the predicted life. This is done by means of the numerically performed profile likelihood and prediction profile likelihood respectively.

The obtained curves after fitting to the experimental results consist of the mean curves for the used data and the selected model. With enough data points from the experiments approximate lower 90% prediction limit can be computed enabling the establishment of a design curve. The 90% prediction limit corresponds to a 95% survival probability. The lower 90% prediction limits are approximations, due to the non-linearity in the used fatigue life models. The accuracy of these limits was nevertheless confirmed by a more thorough investigation based on the prediction profile likelihood method.

5.2.2 ASME design curve for welds

The ASME design curve is obtained through adjustment of the ANL mean curve obtained from experimental data on smooth specimens. The adjustment is illustrated in more detail in Figure 1 and is intended to take transferability into account, i.e. the transfer from smooth test specimen to a component. The ASME design curve presented in Figure 1 is used in conjunction with local or peak strain amplitudes. The curves to be used in conjunction with nominal strain amplitudes are obtained through reduction with a factor K, also designated as fatigue reduction factor, in order to consider the presence of a weld or a notch. For welds, this factor is denoted the *weld reduction factor*. The reduced ASME design curve and ANL mean curve can then be used in conjunction with the nominal strain amplitude. Figure 9(a) illustrates the difference between adjustment and reduction of the studied SN curves.

The considered piping components include a circumferential welding joint in as-welded condition, which results in altered fatigue strength when compared to a smooth component without welding joint. The presence of the weld yields a reduction of the fatigue resistance. Possible fatigue crack initiation is further promoted by the as-welded condition of the weld due to the induced strain concentration locally at the weld toe. The local strain at the weld toe is larger than the nominal strain recorded during testing. Plastic yielding will consequently first occur at the weld toe, when the nominal strain is still elastic. The weld fatigue reduction factor K for the considered piping component is in short required to allow comparison between the experimental results based on nominal strain amplitudes and the SN curves derived for smooth specimens or components used in conjunction with local strain amplitudes. The latter are reduced by means of K as illustrated in Figure 9(a) to allow use with nominal strain amplitudes.

An accurate estimation of the weld fatigue reduction factor K of the investigated piping components would require an additional experimental investigation: fatigue testing of the investigated piping components without a circumferential welding joint. The weld fatigue reduction factor for welding joints in piping components is

namely affected by various parameters, see [16] for more detail. In the current investigation K was however estimated with two analytical approaches. These estimates of the weld fatigue reduction factor do implicitly assume a dominant contribution of geometrical effects.

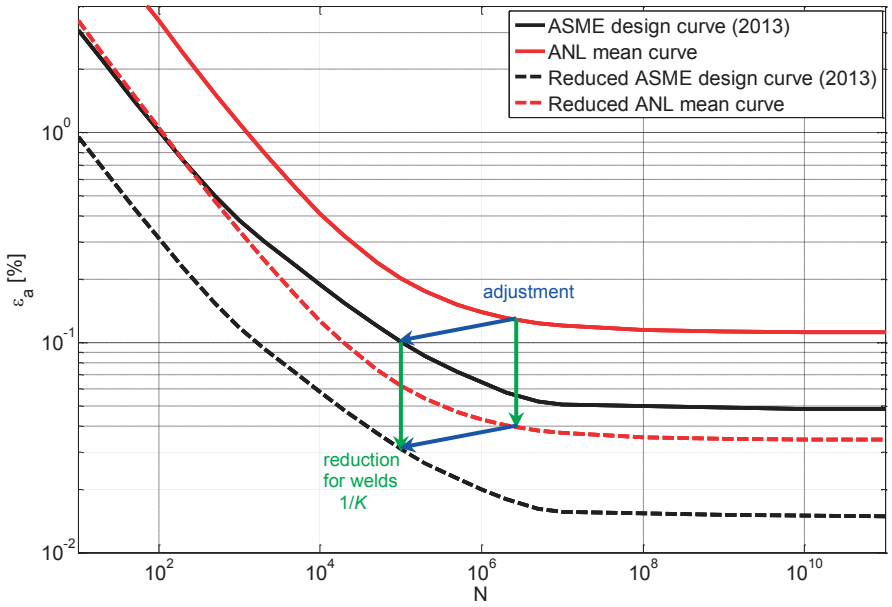

(a) Illustration of the weld fatigue reduction with factor K = 3.24 to account for the presence of a weld and use with the nominal strain amplitude.

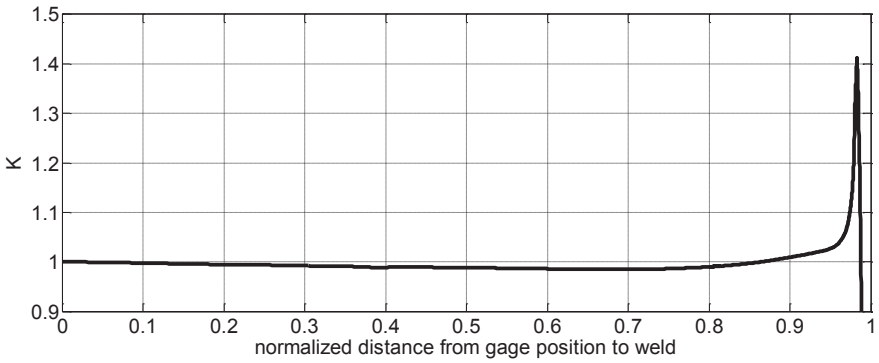

(b) Strain concentration factor computed with FE model of welded piping component. Element size near the weld toe was approximately 0.1 mm.

Figure 9. Effects of weld on (a) SN curves and (b) strain field.

5.2.2.1 ASME approach

The relation between the peak strain amplitudes and nominal strain amplitudes can be derived assuming linear elasticity and NB-3653.2 in [1], where the peak stress is related to the nominal stress by means of stress indices K_2 and C_2. The local stress index K_2 represents a local concentration factor, whereas the secondary stress index C_2 corresponds to a correction related to the thickness of the piping component. Hence a measure of the weld fatigue reduction factor is then estimated as $K = K_2 C_2$. For the investigated piping component subjected to bending, the stress indices are $K_2 = C_2 = 1.8$, according NB-3680 in [1], yielding $K = 3.24$.

5.2.2.2 Numerical approach

A potential alternative approach is to compute an elastic strain concentration factor for the investigated pipe geometry with a weld geometry given by a cap height of 0.5 mm and weld toe radius of 1 mm, with a finite element (FE) simulation using ANSYS 14.5 [17]. The strain concentration factor is then assumed to give an estimate of the weld fatigue reduction factor K [16]. The elastic strain concentration factor was estimated to be 1.4, see Figure 9(b), where the computed strain was normalized with the calculated strain at the gage position, which was assumed to correspond to the nominal strain. The elastic strain concentration factor is however a non-conservative measure for quantifying the magnitude of the local strain at the weld toe, when non-linear material behavior is present. Direct measure the actual local strain at the weld toe is experimentally very difficult and predictions using FE simulations would require the use of more advanced material models, which also show some limitations [18].

6 Results

6.1 Preliminary investigation

6.1.1 Non-linear material behavior

During fatigue testing of the austenitic SS some non-linear behavior could be observed already in the elastic strain range, i.e. for strains smaller than the yield strain $\varepsilon_Y = 0.141\%$. The moment-nominal strain diagram exhibited clear hysteresis loops, as illustrated in Figure 10 for a CA fatigue test at 2.8 mm prescribed displacement amplitude. The moment was calculated from the recorded force and the moment arm equal to 300 mm introduced by the fixtures. For spectrum loads the hysteresis loops do not superimpose, as different amplitudes are included. The presence of hysteresis was therefore illustrated here for CA data.

The size of the hysteresis loops increased clearly with maximum nominal strain amplitude, as illustrated in Figure 11(a). The computed total area corresponds to the area of the envelope around the hysteresis loops occurring during one period. Another feature of the moment-nominal strain diagram is the overall slope k_M computed by the least square method using data corresponding to one period. A clear decrease of the slope with increasing maximum nominal strain amplitude can be observed in Figure 11(b). These results indicate the presence of non-linear material behavior during fatigue testing, not only for nominal strain amplitudes exceeding the yield strain. Note that for the considered loads the maximum strain amplitudes at the weld toe did exceed the yield strain due to the strain concentration.

The effects of friction in the experimental set-up were evaluated and considered to be negligible when compared to the hysteresis due to non-linear material behavior. Some minor contribution of friction could be observed at load reversals, where the hysteresis loops could show a tiny local loop. This effect was related to friction arising in the connection between fixture and testing machine. The effect of friction was minimized through lubrication of the connection. Furthermore, an estimative and conservative calculation confirmed very little influence of friction. It was consequently ensured that the observed hysteresis is predominantly due to non-linear material behavior.

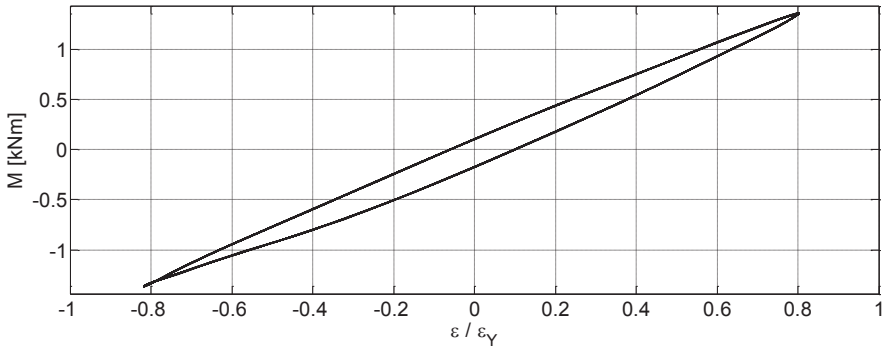

Figure 10. Hysteresis loops in the moment-nominal strain diagram obtained for component 26 during 10 s of testing.

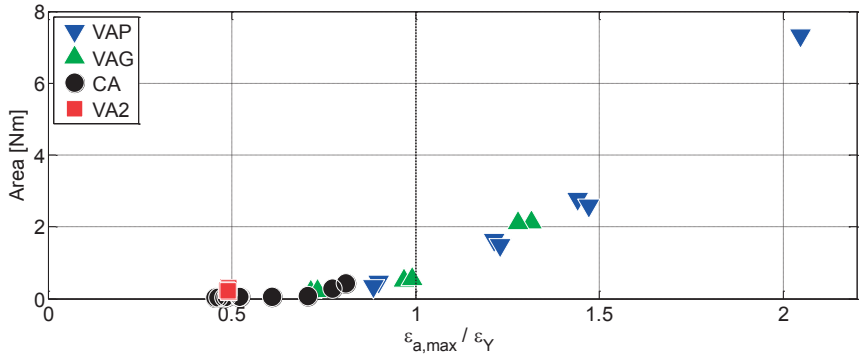

(a) Total area vs normalized maximum nominal strain amplitude.

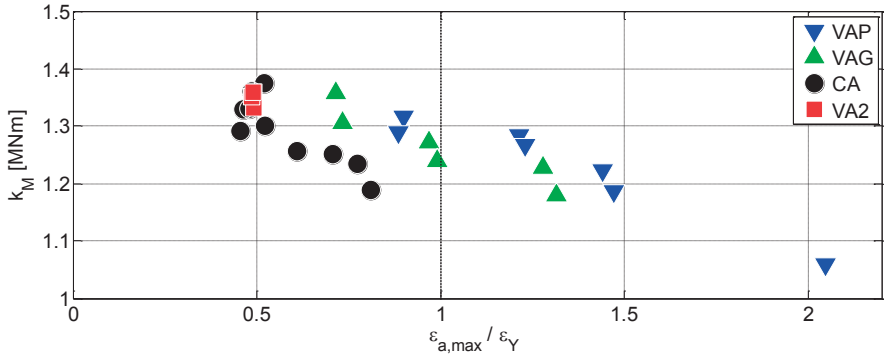

(b) Overall slope vs normalized maximum nominal strain amplitude.

Figure 11. Characteristics of the hysteresis loops in the moment-nominal strain diagram for one period for each of the experiments, evaluated near the start of the fatigue experiment.

6.1.2 Mean nominal strain due to internal pressure in the piping component

The internal pressure in the welded piping component generates an axial strain which was estimated to $\varepsilon_0 = 0.0054$ % for an internal pressure of 70 bar. Figure 12 illustrates the evolution of the average axial strain during pressurization and depressurization of a piping component. The average axial strain was computed from four strain measures used during pre-testing.

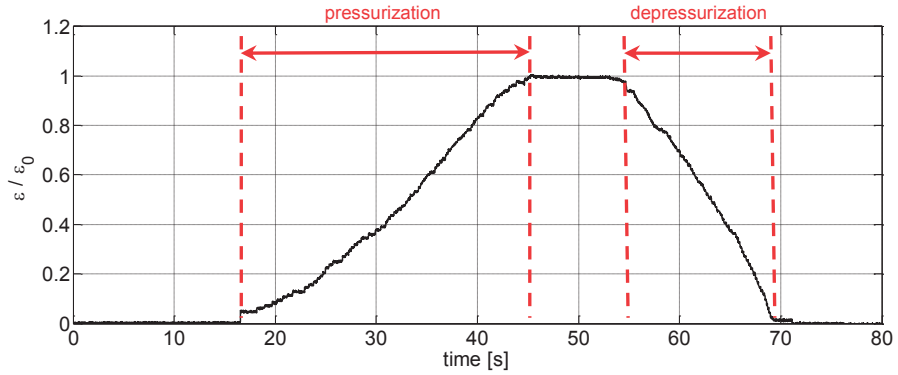

Figure 12. Normalized average axial strain during pressurization and depressurization of the welded piping component to 70 bar.

6.2 Experimental fatigue results

The results for the 28 fatigue experiments are summarized in Figure 13 and Table 4. The total number of strain cycles ranges between 100000 and more than 5 million cycles. Experiments at the upper limit of this range corresponded to run-outs, i.e. the fatigue tests were stopped prior to leakage. This was the case for pipes 13, 16, 22, 29 and 30. The total number of strain cycles to which each tested piping component was subjected is denoted N, including also strain cycles with small strain amplitudes contained in the VAP and VAG load spectra. The different equivalent strain measures were computed once the model parameters were estimated, see Section 6.2.3. The total number of strain cycles actually causing fatigue damage according to the Langer model is given by N_C. This quantity was computed by only considering the strain cycles to failure with amplitudes exceeding the constant fatigue limit C, hence $n = N_C$ when considering the entire load sequence until failure of the component. The BC-norm strain and N_C are directly related. $N_C < N$ for the VA data points which would correspond to a shift leftwards in Figure 13(c), when only the number of cycles actually causing fatigue damage would be considered instead of the total number of cycles to failure. Similarly the total number of cycles causing fatigue damage according to the DFL model is given by N_c.

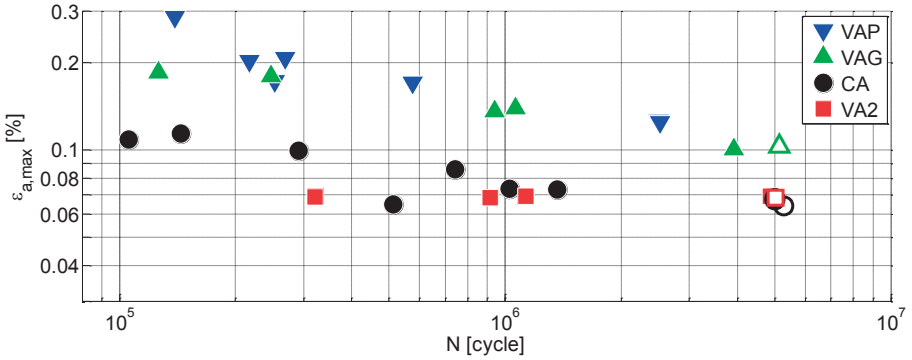

(a) Maximum nominal strain amplitude vs total number of cycles to failure.

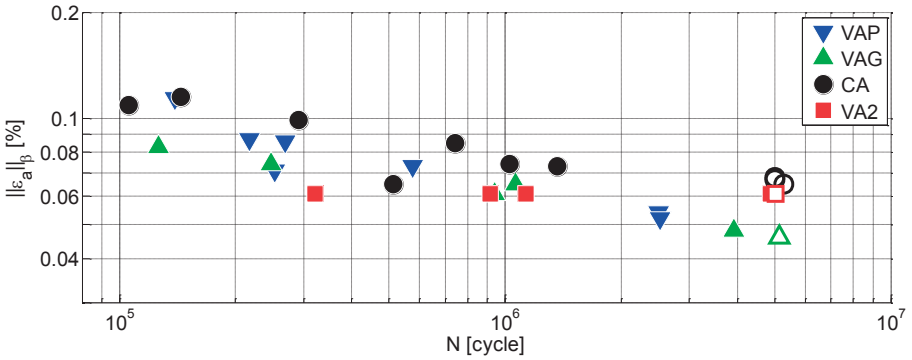

(b) Beta norm strain with β = 4.6 vs total number of cycles to failure.

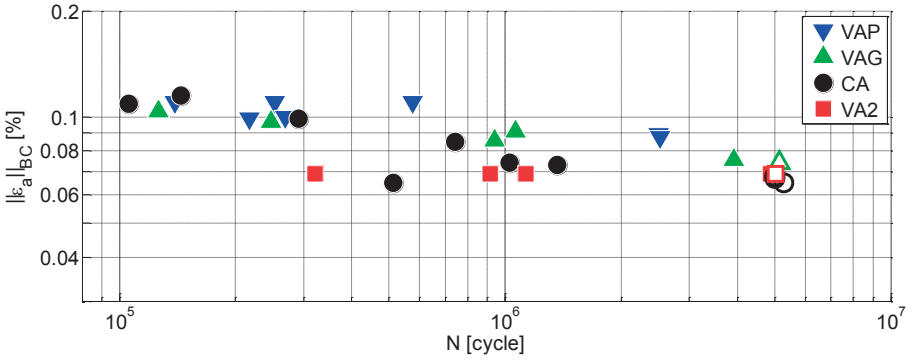

(c) *BC*-norm strain with B = 2.01 and C= 0.058% vs total number of cycles to failure $N > N_C$.

Figure 13. Experimental results from the 28 fatigue experiments on welded piping components using different load spectra and severity. The empty markers indicate run-outs.

Table 4. Experimental results from performed fatigue tests. The beta-norm was computed with β = 4.6 and the BC-norm with B = 2.01 and C = 0.058%. The strain measures are all based on the recorded nominal strain.

Pipe ID	Load type	Severity(*)	N [cycles]	max ε_a [%]	$\|\|\varepsilon_a\|\|_\beta$ [%]	$\|\|\varepsilon_a\|\|_{BC}$ [%]	N_C [cycles]	N_c [cycles]
1	VAP	Medium	575000	0.171	0.073	0.1100	61000	110000
2	VAP	Low	2500000	0.126	0.054	0.0894	200000	280000
3	VAP	High	217000	0.203	0.087	0.0988	72000	72000
4	VAP	Peak	139000	0.288	0.114	0.1100	69000	32000
5	VAP	Low	2520000	0.124	0.052	0.0875	190000	310000
6	VAP	Medium	253000	0.173	0.071	0.1100	25000	130000
7	VAP	High	269000	0.207	0.086	0.0998	80000	72000
8	VAG	Medium	941000	0.136	0.061	0.0858	180000	230000
9	VAG	Medium	1063624	0.140	0.065	0.0912	200000	180000
10	VAG	High	126350	0.185	0.083	0.1040	34000	79000
11	VAG	Low	3921275	0.101	0.048	0.0756	380000	510000
(†)13	VAG	Low	5133411	0.103	0.046	0.0740	470000	580000
14	VAG	High	247441	0.180	0.074	0.0970	63000	120000
15	CA	2.2	740735	0.085	0.085	0.085	740735	740735
(†)16	CA	1.7	5269515	0.065	0.065	0.065	5269515	0
18	CA	1.95	1027847	0.074	0.074	0.074	1027847	0
19	CA	2.6	291260	0.099	0.099	0.099	291260	291260
20	VA2	-	1131716	0.069	0.061	0.069	565858	0
21	VA2	-	4880396	0.069	0.061	0.069	2440198	0
(†)22	VA2	-	5024628	0.068	0.061	0.069	2512314	0
23	VA2	-	913856	0.069	0.061	0.069	456928	0
24	VA2	-	321904	0.069	0.061	0.069	160952	0
25	CA	2.8	105769	0.109	0.109	0.109	105769	105769
26	CA	2.8	144230	0.115	0.115	0.115	144230	144230
27	CA	1.8	1367448	0.073	0.073	0.073	1367448	0
28	CA	1.7	512749	0.065	0.065	0.065	512749	0
(†)29	CA	1.7	5000000	0.068	0.068	0.068	5000000	0
(†)30	CA	1.7	5000000	0.067	0.067	0.067	5000000	0

(*) The severity for the CA experiments corresponds to the prescribed displacement amplitude.

(†) Run-out experiment, where the number of cycles exceeded the run-out limit of 5 million cycles. The fatigue tests were stopped prior to leakage.

6.2.1 Leakage and fatigue crack growth

The piping component was water-pressurized which allowed for the failure criterion based on leakage. The presence of water drops near the circumferential butt weld was an illustration of onset of leakage, see Figure 14, indicating the presence of a propagating fatigue crack. Water contact during some part of the damage process is inevitable. The maximum nominal strain occurs at the outside, which makes outside initiation most likely. However, it has not been verified if the crack initiated from the outside. Several necessary conditions for environmental fatigue are not fulfilled [2] and environmental effects should therefore be very small for long lives in room temperature at relatively high frequency. Potential environmental effects on the test results were hence assumed negligible. Higher temperature and slower load application should certainly be required in order to examine environmental effects for potential inside crack initiation. Figure 15 illustrates fatigue cracks at a later stage of the fatigue test. A fatigue crack has propagated in a circumferential direction in the heat affected zone (HAZ) of the weld.

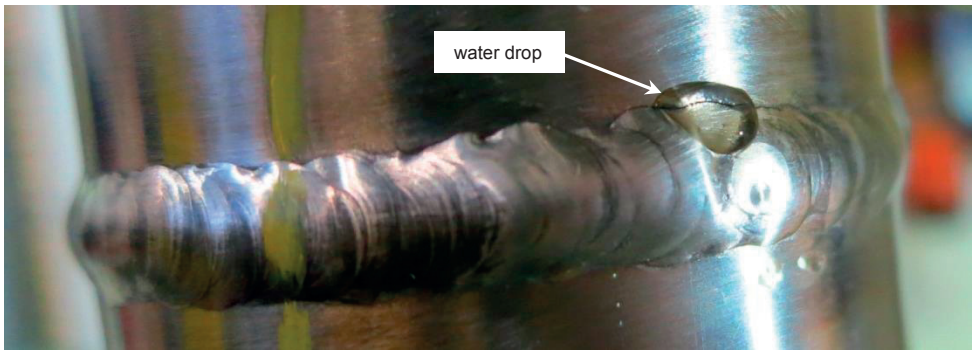

Figure14. Illustration of visual detection of onset of leakage during final stage of fatigue testing.

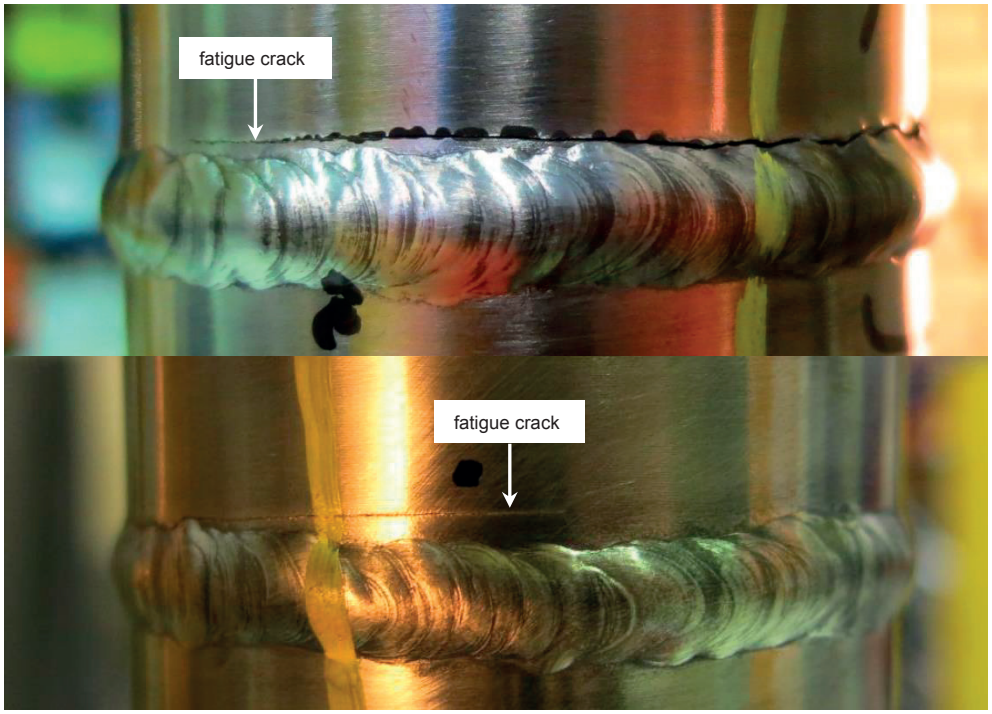

Figure 15. Illustration of fatigue crack propagation in circumferential direction during final stage of fatigue testing.

6.2.2 Strain measures

Table 4 includes different strain measures informing about different aspects of the fatigue load. The maximum nominal strain amplitude informs about whether the spectrum loads included strain cycles yielding plastic deformation at the gage position. The majority of the strain cycles in each load block of the VAP and VAG spectra had small nominal strain amplitudes, see Figure 6. The equivalent strain measures take this feature of the fatigue load into account, resulting in lower values. The equivalent strain measures are therefore more appropriate as fatigue parameters for VA loading. The maximum strain amplitude describes one or a few extreme load cycles, but all information about the remaining cycles in the load spectrum is lost. Figure 13(a) presents the experimental fatigue life as function of the maximum nominal strain amplitude yielding high values for the VA tests, when compared to the representation using the β-norm strain in Figure 13(b) or the *BC*-norm strain in Figure 13(c).

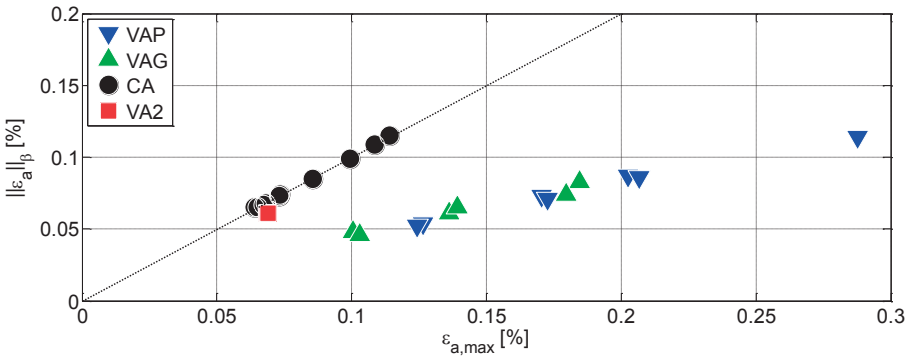

(a) β-norm strain with β = 4.6.

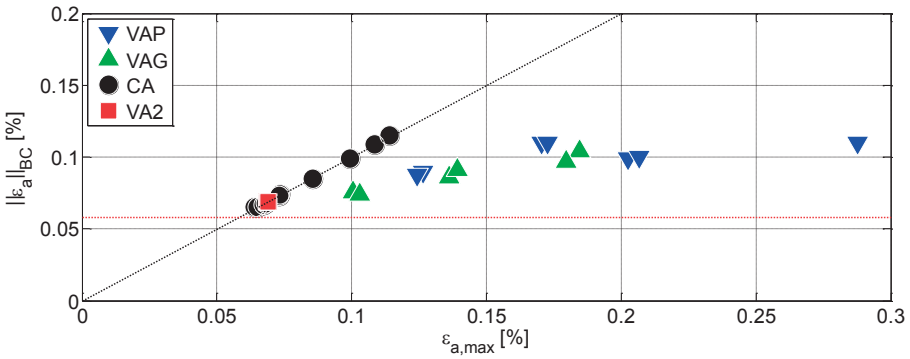

(b) *BC*- norm strain with *B* = 2.01 and *C*= 0.058%, the latter being represented by the red dotted line.

Figure 16. Equivalent nominal strains vs maximum nominal strain amplitude for the different fatigue tests. The first bisectrix is presented as a black dotted line.

The relation between the equivalent nominal strain measures and the maximum nominal strain amplitude is illustrated in Figure 16. The CA data points are always situated on the first bisectrix, as the equivalent strain measures for CA loading always yield the nominal strain amplitude. The equivalent strain measures as function of the maximum nominal strain amplitude tend to show alignment of the VAP and VAG data points, but with a more shallow slope. For the β-norm strain, see Figure 16(a), a linear relation can be extrapolated to zero. In the case of the *BC*-norm, see Figure 16(b), the relation intersects the first bisectrix at the constant fatigue limit *C* and will not extrapolate to zero. The VAP data points in Figure 16(b) also illustrate the non-monotonic behavior of the selected *BC*-norm definition, see Eq. (6). For increased maximum strain amplitude, not only the strain amplitudes are increased, but also the total number of strain cycles in the load spectrum actually contributing to fatigue damage, *n*, which may result in an actual decrease of the equivalent *BC*-norm strain, yielding the non-linear behavior observed here. Linearity is recovered with the alternative *BC*-norm strain based on a normalization using the constant total number of strain cycles included in a load sequence.

6.2.3 Parameter estimation

The estimated parameters for each one of the three investigated fatigue life models are presented in Table 5. The parameter estimation was here performed using the data from both the VAP and VAG experiments. The VA data was grouped as separate treatment yielded similar results. For the Basquin relation only two parameters are to be estimate, α and β, whereas the parameters in the Langer equation are *A*, *B* and *C*. The model with decreasing fatigue limit (DFL) does also include three parameters. The estimated standard deviation of the random error in the logarithmic fatigue life is denoted $\hat{\sigma}$, it is therefore approximately equal to the coefficient of variation of the fatigue life. For the three parameter models, the Langer model yields a better fit with the experimental data than the DFL model, given the smaller estimated standard deviation.

Table 5. Estimated model parameters and standard deviation of the random error based on VAP and VAG data.

Model:	Factor		Slope		Fatigue limit		$\hat{\sigma}$
Basquin	$\hat{\alpha}$	2.89	$\hat{\beta}$	4.6	-		0.42
Langer	$\hat{A}$	128	$\hat{B}$	2.01	$\hat{C}$	0.058 %	0.36
DFL	$\hat{a}$	3.51	$\hat{b}$	4.45	$\hat{c}$	0.076 %	0.42

The estimated value for β was previously used in the β-norm strain measures computed in Table 4. Similarly the estimates for *B* and *C* were used for the *BC*-norm strain measures. These norms used the nominal strain amplitudes which were recorded during the fatigue experiments. Note also that the estimated fatigue limits in Table 5 are intended for use in conjunction with the nominal strain.

6.2.4 Predicted number of load cycles causing fatigue damage

The three studied fatigue models differ in their way of taking the fatigue limit into account. The Basquin model has no fatigue limit, thus any strain cycle contributes to generate fatigue damage. The ratio of the predicted number of load cycles causing fatigue damage and the total number of load cycles during a test is for the Basquin model always equal to unity. However for the remaining models the presence of a fatigue limit will yield lower ratios for the VA tests, in particular.

Figure 17(a) presents the ratio N_C/N based on the Langer model, where N_C represents the number of strain cycles with strain amplitudes exceeding the constant C, and is tabulated in Table 4. Similarly the ratio based on the DFL model is shown in Figure 14(b) and is computed as N_c/N, where N_c, see Table 4, is the actual number of strain cycles causing fatigue damage using the decreasing fatigue limits. For experiments with maximum nominal strain amplitude smaller than the estimated initial fatigue limit, no fatigue damage will develop, hence a zero ratio. For the CA data points the ratio always equals unity, when the strain amplitude exceeds the fatigue limit. For the VAP and VAG data points, the general trend indicates increasing ratios for fatigue tests with shorter fatigue lives, i.e. with larger maximum strain amplitudes. For larger maximum strain amplitudes, more strain cycles are namely committed in the development of fatigue damage. The differences in behavior between the VAP and VAG data points are related to the differences in the load spectra, see for instance the level crossing diagrams in Figure 6. The data points for VA2 represent only one severity, hence a constant ratio for each model.

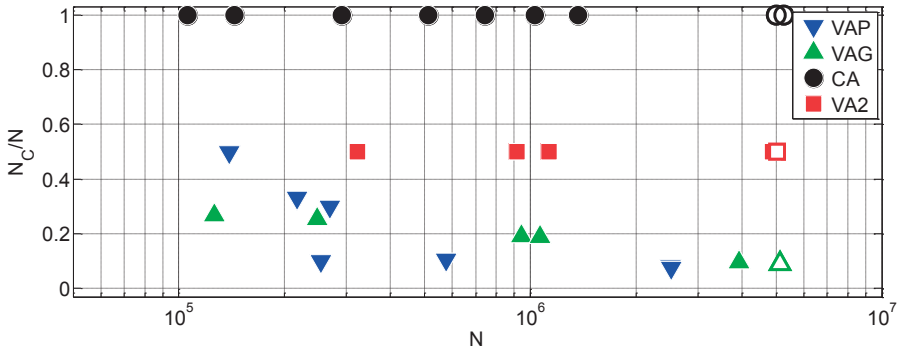

(a) Predicted N_C/N ratio with the Langer model using the constant fatigue limit C = 0.058%.

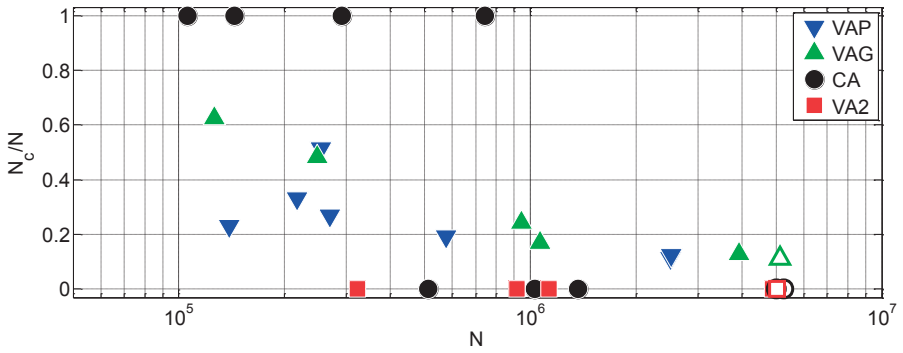

(b) Predicted N_c/N ratio with the DFL model with initial fatigue limit c = 0.076%.

Figure 17. Predicted percentage of load cycles causing fatigue damage for the fatigue models with non-zero fatigue limit. The empty markers represent run-outs.

Based on the VAP and VAG data, the estimated initial fatigue limit for the DFL model is significantly higher than the constant fatigue limit in the Langer model, see Table 5. This explains why the DFL model predicts no fatigue damage for VA2 and CA fatigue tests, which eventually failed prior to the run-out limit. The DFL model yields therefore non-conservative predictions for these experiments.

6.2.5 Comparison with reduced ASME design curve (for welds)

The 90% prediction limits for each fatigue model corresponding to 95% survival probability are interpreted as design curves specifically obtained from the performed experiments, namely with VAP and VAG load spectra. These experimental design curves are compared to the reduced ASME design curve which accounts for the presence of a welding joint. Both a weld fatigue reduction factor K equal to 3.24, as proposed by ASME and 1.4, as obtained through a simplified FE analysis, are considered. The reduced ANL curve is representing the mean curve for test specimens with a welding joint.

6.2.5.1 Basquin model

The dashed lines in Figure 18 correspond to the mean curves, whereas solid lines represent the lower 90 % prediction limit for the Basquin model or the design curve. The black solid curve is the corresponding reduced ASME design curve. The black markers correspond to the experimental data points used for the estimation of the different model parameters. The differences between Figures 18(a) and (b) solely depend on the used weld fatigue reduction factors.

Figures 18(a) illustrates the considerable conservatism in the ASME approach to transferability, as for the whole considered range of fatigue lives, the lower 90% prediction limit of the Basquin model is always situated above the reduced ASME design curve. The difference is considerably reduced for K=1.4, in Figure 18(b). ASME assumes the existence of a fatigue limit, whereas the Basquin equation has no fatigue limit, hence the comparison for extended fatigue lives is not relevant. The Basquin model will ultimately yield non-conservative results when compared to ASME's design curve.

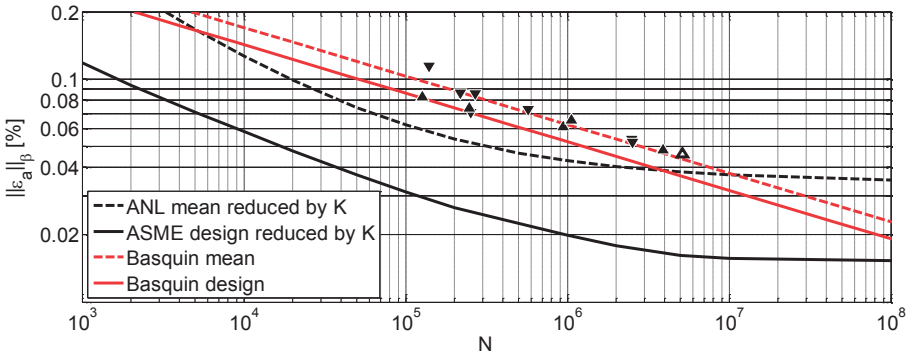

(a) Weld fatigue reduction factor *K*=3.24.

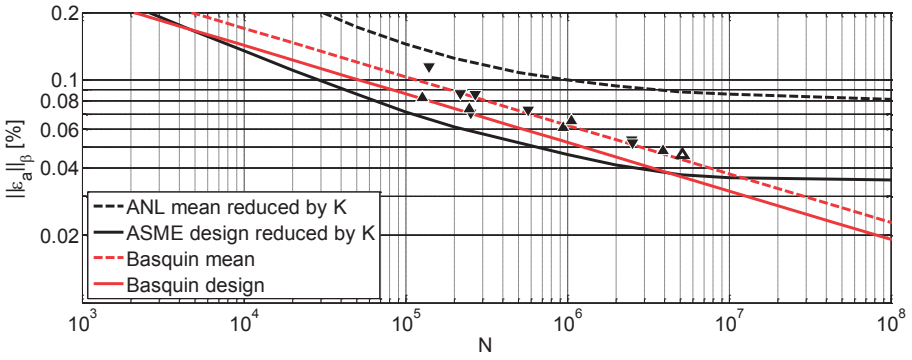

(b) Weld fatigue reduction factor *K*=1.4.

Figure 18. Comparison of the reduced ASME design curve and predictions of the fitted Basquin model.

6.2.5.2 Langer model

The use of the Langer model to investigate the margins in the ASME design curve is consistent, as the ANL curve from which the ASME design curve was derived, is also based on the Langer model. The dashed lines in Figure 19 correspond to the mean curves, whereas solid lines represent the lower 90 % prediction limit for the Langer model or the design curve. The black solid curve is the corresponding reduced ASME design curve accounting for the presence of a welding joint. The black markers correspond to the experimental data points used for the estimation of the different model parameters. Note that the experimental data points are plotted using the total number of cycles actually causing fatigue damage, i.e. N_C. The differences between Figures 19(a) and (b) solely depend on the used weld fatigue reduction factors.

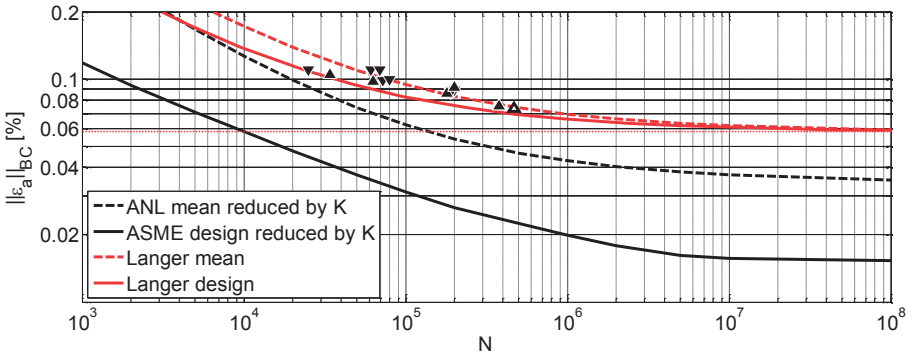

(a) Weld fatigue reduction factor *K*=3.24.

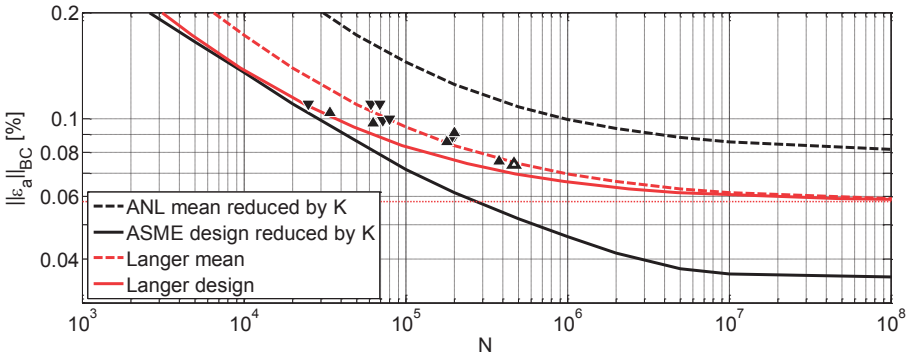

(b) Weld fatigue reduction factor *K*=1.4.

Figure 19. Comparison of the reduced ASME design curve and predictions of fitted Langer model. The horizontal dotted line represents the fatigue limit *C*.

Figures 19(a) illustrates again the considerable conservatism in the ASME approach to transferability, as for the whole considered range of fatigue lives, the lower 90% prediction limit of the Langer model is always situated far above the reduced ASME design curve. It is even predominantly situated above the reduced ANL curve. The conservatism is considerably reduced, but preserved, for *K*=1.4, see Figure 19(b). The fitted mean and lower 90% prediction limit are now situated in between the reduced ANL curve and ASME design curve. Large conservatism is preserved at HCF, however for LCF the lower 90% prediction limit of the Langer model nearly coincides with the ASME design curve.

6.2.6 Additional results from CA and VA2 data

The model parameters for the three fatigue models were also estimated based on the CA data, see Table 6. The fatigue limit for the DFL model was however estimated separately from failure/run-out results and the Basquin parameters were then estimated using only results exceeding this fatigue limit. The CA data appeared to yield non-conservative predictions compared to the results based on the VAP and VAG spectra, partly due to the larger estimate of β, see Table 6.

Table 6. Estimated model parameters and standard deviation of the random error based on CA data.

Model:	Factor		Slope		Fatigue limit		$\hat{\sigma}$
Basquin	$\hat{\alpha}$	0.297	$\hat{\beta}$	5.92	-		0.81
Langer	$\hat{A}$	10.4	$\hat{B}$	4.28	$\hat{C}$	0.00096 %	0.49
DFL	$\hat{a}$	1.99	$\hat{b}$	5.07	$\hat{c}$	0.066 %	0.26

The VA2 was initially constructed to allow discrimination of the three used fatigue models. Since the models differ in the way they include the fatigue limit, it was found that a two-level spectrum (VA2) would be sufficient. The levels were chosen so as to give different fatigue life predictions. The high level was chosen between the estimates of C and c in Table 5, whereas the lower level was selected to be lower than the estimated (initial) fatigue limits. Using the three fatigue models, the predicted fatigue lives were then $1.2\ 10^6$, $2.2\ 10^6$ and infinity, for the Basquin, Langer and DFL models respectively. The results from the five VA2 experiments presented unfortunately too large scatter to allow a successful discrimination of the investigated fatigue models. The discrimination of the fatigue models failed partly because of the restraint to have a reasonable testing time. This limitation could be overcome with fatigue testing at even higher frequencies and a load spectrum yielding even larger differences in fatigue life prediction.

The CA and VA2 results are further discussed in [19].

7 Discussion

The difficulties of transferring smooth specimen data has been discussed in a previous SSM-report [3] by Inspecta Technology, in which margins was discussed on basis of a literature study. The proposal of a component test was strongly suggested, not the least due to the complex behavior of austenitic stainless steel even for long lives. Some of the previous conclusions from the literature study [3] are summarized below:

i. Secondary cyclic hardening is decisive for HCF in constant amplitude testing in strain control. This phenomenon is likely to disappear under variable load.

ii. HCF for austenitic steels is determined by its complex elasto-plastic behavior.

iii. The control mode, load or displacement, is important for fatigue.

iv. Residual stresses are likely to relax under loading even in the HCF regime [20].

v. It is shown that using strain amplitude as the only fatigue governing parameter, as in ASME, is inaccurate. A better agreement is obtained by using combined measures involving both stress and strain.

All these conclusions are based on empirical observation and important for practical applications, but escape any consistent and accurate phenomenological explanation. A typical example is the observed and large difference between load and deformation control, which is extremely complex. Another example is secondary hardening, which differs between material batches, and is assumed to have impact on long lives at constant amplitude but assumedly disappear at variable amplitude. The nature of these phenomena is on-going research, and the state of the art research is further summarized in [3]. It is argued that the only way to get a fair control of these effects, and, in fact, the margins in a fatigue application is to preform fairly realistic tests on components. The impact of these effects will be contained within the experiments without requiring uncertain explanations and quantifications. Hence, what can seem to be too much speculation about reasons for the observations for the current work is by purpose avoided and left for more fundamental and future studies of the basis of fatigue.

A series of fatigue tests on welded piping components was performed under realistic testing conditions, i.e. with internal pressure and VA loading, as opposed to the classic CA fatigue tests performed on smooth test specimens. The newly developed experimental set-up allowed for flexible testing of the piping components at relatively high frequencies.

The main focus of the experimental series was the HCF regime, however in order to improve the fitting of the different fatigue models, tests were also performed at LCF. Different load spectra were investigated in order to differentiate the predictions of the investigated fatigue models, hereby motivating the use of different load spectra. Table 5 supports the Langer model, but it is difficult to draw a more general conclusion on which model is best, as the discrimination based on the VA2 spectrum failed [19]. The Basquin model lacking a fatigue limit will lead to very conservative predictions, even more conservative than ASME when considering very small strain amplitudes. How realistic these predictions then are is another question. The Langer and DFL models include a fatigue limit. However these predictions are then largely dependent of the estimated fatigue limit parameter. An advantage of the Langer model is its consistency with the ASME design curve, as the latter is derived from the ANL mean curve, which was fitted

with a Langer equation. Note however that the Langer equation was initially actually proposed for LCF [14].

The ASME margins were estimated by comparing a reduced ASME design curve for use in conjunction with nominal strain amplitudes and the experimental 90% prediction limits for both the Basquin and Langer fatigue life models. These prediction limits correspond to 95% survival probability and are interpreted as experimental design curves. The ASME design curve is mainly based on CA data with smooth test specimens, whereas the current estimated prediction limits were computed based on VA data with welded piping components. The ASME design curve for welds (weld reduced) was conservative, as it constitutes a lower bound when compared to the fitted design curves for relevant fatigue life range. The mean curves from the fatigue models and the experimental data points are not coinciding with the weld reduced ANL mean curves, which illustrates the need for a transferability correction to take amongst others differences in load and geometry into account. The over-conservatism of the ASME fatigue procedure to transferability resulted in a design curve well below the predicted 95% survival probability curves for the Langer model. The ASME design curve does therefore seem to correspond to a significantly larger survival probability than 95% for the investigated piping component. This observation is consistent with a decreased adjustment factor for number of cycles, 10 instead of 12, proposed in a preliminary revised version of the ANL report [2].

The extent of the margins depends clearly on the value of the weld fatigue reduction factor *K,* used to reduce the original ASME design curve tabulated in [1]. The margins are considerably reduced with a smaller value, such as the one obtained from a linear elastic FE analysis.

The experimental results did indicate the presence of non-linear material behavior even at small strain amplitudes; see results in Figures 10 and 11. This non-linear behavior makes it more challenging to predict the actual local strains at the weld toe, affecting directly the estimation of the weld fatigue reduction factor *K* to be used. An experimental investigation with fatigue tests using unwelded piping components should improve the estimation of the particular *K* for the investigated piping components.

Due to the derivation of experimental design curves, the margins of the ASME design curve may be evaluated outside the investigated fatigue life range. These margins are very conservative in the region of the run-out limit and above, see Figure 19. These results may however be uncertain, due to the lack of data points and the significant effect of the estimated fatigue limit parameter on the experimental design curves. The relation between the experimental mean and design curves is based on the distribution of the fatigue life, resulting in a horizontal shift. In the case of the Langer model, the mean and design curves have consequently the same asymptotic fatigue limit, see Figure 19. The uncertainty of the estimated fatigue limit has then a direct effect on the evaluation of the ASME margins at HCF. Comparison with design curves based on the Basquin model in this region is not relevant due to lack of a fatigue limit.

The obtained results are particular to the investigated components and their geometry. The fatigue life of the component was for instance defined by leakage, which is directly related to the wall-thickness of the component. Piping components with different wall-thicknesses would therefore exhibit different fatigue lives than those obtained with the current experimental study. Similarly pipes with different diameter would be subjected to different bending loads, resulting in different nominal strains. The ASME approach to transferability was shown to yield a conservative design curve for different types of load spectra. The current experimental study showed nevertheless that fatigue testing of a component

with a known load spectrum will yield less conservative, but realistic design curves with user-defined survival probability.

Fatigue testing with a realistic load spectrum for the considered application is important to obtain conservative and precise experimental design curves. CA testing may result in longer lives. The type of loading history also influences the fatigue limit [2], hence the importance of testing with realistic loads when deriving experimental design curves for use at HCF.

8 Conclusions

The current study aimed at making up for the shortcoming of experimental data on realistic austenitic stainless steel components, with particular focus on HCF and variable amplitude loading. Fatigue experiments were performed at both LCF and HCF up to a run-out limit of $5\ 10^6$ cycles. Both constant amplitude and three different load spectra were applied during the fatigue tests. The obtained results and/or findings of the performed investigation are as follows:

- The experimental study allowed increased understanding of the margins in ASME, especially for HCF, which previous component testing at LCF could not provide.
- For the investigated piping component the ASME design curve represented a survival probability in excess of 95 % for realistic load spectra.
- The results indicate extensive conservatism in the ASME approach to deal with transferability. This result was obtained with weld fatigue reduction factors implied by ASME or estimated by an FE analysis. The extent of the margins did however largely depend on this factor, for which an accurate estimate is difficult due to the non-linear material behavior observed.
- More precise fatigue life predictions could be obtained with an experimental test series, despite the relative lack of generality and additional experimental efforts. Experimentally based design curves can then be determined yielding more realistic margins.
- The approach should be based on realistic VA loading to preserve conservatism, as the type of loading affects the fatigue life. The CA results indicated namely non-conservatism.
- No differences could be detected between the empirical piping spectrum and the synthetic Gaussian spectrum, which suggests that the determination of VA-strength probably could be standardized to a certain synthetic spectrum type.
- Different fatigue models may be used in the evaluation of the test results and the derivation of design curves. The Basquin model is easy to use with conservative predictions, especially at HCF, however is limited due to the lack of a fatigue limit yielding over-conservatism. The Langer model showed best agreement with the variable amplitude data and is furthermore consistent with ASME.

The experimental investigation resulted in design curves for the studied austenitic SS piping component corresponding to 95% survival probability for use with a piping or a Gaussian load spectrum. These design curves with more precise margins contribute to the control of potential fatigue risks linked to the investigated welded piping component.

9 Recommendations

The performed investigation dealt with a specific welded piping geometry which was fatigue tested under specific loading conditions using a limited number of test specimens. The observed limitations of the study can to some extent be resolved considering the following actions:

- The actual initiation site of the fatigue cracks was not verified by closer investigation of the fracture surfaces, which requires breaking up the test specimens. This minor experimental study would yield valuable information and allow validation of the assumed fatigue crack initiation at the outer surface of the welded piping component, which improves knowledge about the damage process in the tested welded component.
- The complex material behavior of austenitic SS, which was observed even at small elastic strain amplitudes, should be further investigated in order to better describe the strains at the weld toe or strain concentration. In the current study the concentration factor was estimated to 1.4, but its direct effect on the extent of the ASME margins supports a more elaborate investigation. A more precise evaluation of the strain concentration can be performed with an FE analysis using a non-linear material model as those proposed in [18].
- Validation of the obtained estimate of the weld fatigue reduction factor can be performed with experimental fatigue testing of unwelded piping components.
- The selection of the most appropriate fatigue model is possible with additional fatigue testing. In the current investigation this differentiation was hampered due to the limited run-out limit and large scatter in the two-level block spectrum results. The use of an increased number of test specimens would allow more detailed investigation of the observed scatter.
- Fatigue testing with further increased testing frequency would allow performing fatigue testing with higher run-out limit within reasonable testing time. Such fatigue tests would contribute to confirm conservatism of the ASME margins even at longer fatigue live. The determination of a fatigue limit would also be enabled.
- The current experimental study is too limited to propose a general modification of the ASME design curve at HCF to avoid over-conservatism. The fatigue testing used a number of 28 test specimens, all with identical geometry. Different realistic piping components and/or additional fatigue tests would contribute to support the findings of the current study and allow generalization.

10 Acknowledgement

The Swedish Radiation Safety Authority, SP Technical Research Institute of Sweden and Ringhals AB are gratefully acknowledged for the financial support, help with manufacturing of the test specimens and performing of the fatigue tests. The austenitic stainless steel seamless pipes used for the test specimens were kindly provided by Sandvik AB.

11 References

[1] ASME, Boiler and Pressure Vessel Code, Section III, Rules for Construction of Nuclear Facility Components, 2013.

[2] O. K. Chopra, W. J. Shack, Effect of LWR Coolant Environments on the Fatigue life of Reactor Materials, NUREG/CR-6909, 2007.

[3] M. Dahlberg, D. Bremberg, Fatigue Margins for Austenitic Stainless Steels in ASME Boiler and Pressure Vessel Code – A Literature Study, SSM-2012:50, 2012.

[4] J. Colin, A. Fatemi, Variable amplitude cyclic deformation and fatigue behaviour of stainless steel 304L including step, periodic, and random loadings, *Fat. Fract. Eng. Mat. Struct.*, 33, 2010, 205 - 220.

[5] J. Heald, E. Kiss, Low cycle fatigue of nuclear pipe components, *J. Press. Vessel Tech.*, 1974, 171 - 176.

[6] X. Lu, Influence of residual stress on fatigue failure of welded joints, North Carolina State University, 2002.

[7] P. Y. Cheng, Influence of Residual Stress and Heat Affected Zone on Fatigue Failure of Welded Piping Joints, North Carolina State University, 2009.

[8] T. Svensson, Fatigue testing with a discrete-time stochastic process, *Fat. Fract. Eng. Mat. Struct.*, 17, 1994, 727 - 736.

[9] K. N. Smith, P. Watson, T. H. Topper, A Stress-Strain Function for the *Fatigue of Metals, J. Mater.*, 1970, 767 - 778.

[10] A. Palmgren, Die Lebensdauer von Kullagern, Zeitschrift des Vereins Deutscher Ingenieure, 1924, 339 - 341, (In German).

[11] M.A. Miner, Cumulative damage in fatigue, *J.Appl. Mech.*, 12, 1945, 159 - 164.

[12] P. Johannesson, T. Svensson, J. de Maré, Fatigue life prediction based on variable amplitude tests - methodology, *Int. J. Fatigue*, 27, 2005, 954 - 965.

[13] O. H. Basquin, The exponential law of endurance tests, Proc. ASTM,10:625-630, 1910.

[14] B. F. Langer, Design of Pressure Vessels for Low-Cycle Fatigue, *ASME J. Basic Eng.*, 84, 389 – 402, 1962

[15] T. Svensson, Cumulative fatigue damage taking the threshold into account, *Fat. Fract. Eng. Mat. Struct.*, 25, 2002, 871- 876.

[16] C. E. Jaske, Fatigue-Strength-Reduction Factors for Welds in Pressure Vessels and Piping, *ASME J. Pressure Vessel Technol.*, 122, 2000, 297-304.

[17] User manual, Release 14.5, ANSYS, Inc.

[18] M. Dahlberg, P. Segle, Evaluation of models for cyclic plastic deformation – A literature study, SSM-2010:45, 2010.

[19] T. Svensson, D. Hannes, P. Johannesson, M. Dahlberg, A. Anderson, Three HCF models for strain fatigue life of welded pipes in austenitic stainless steel, *Proc. Eng.*, 101, 2015, 476-484.

[20] J. Colin, A. Fatemi, S. Taheri, Fatigue Behavior of Stainless Steel 304L Including Strain Hardening, Prestraining, and Mean Stress Effects, *J. Eng. Mater. Technol.*, 132(2), 2010, 1-13.

2015:38

The Swedish Radiation Safety Authority has a comprehensive responsibility to ensure that society is safe from the effects of radiation. The Authority works to achieve radiation safety in a number of areas: nuclear power, medical care as well as commercial products and services. The Authority also works to achieve protection from natural radiation and to increase the level of radiation safety internationally.

The Swedish Radiation Safety Authority works proactively and preventively to protect people and the environment from the harmful effects of radiation, now and in the future. The Authority issues regulations and supervises compliance, while also supporting research, providing training and information, and issuing advice. Often, activities involving radiation require licences issued by the Authority. The Swedish Radiation Safety Authority maintains emergency preparedness around the clock with the aim of limiting the aftermath of radiation accidents and the unintentional spreading of radioactive substances. The Authority participates in international co-operation in order to promote radiation safety and finances projects aiming to raise the level of radiation safety in certain Eastern European countries.

The Authority reports to the Ministry of the Environment and has around 300 employees with competencies in the fields of engineering, natural and behavioural sciences, law, economics and communications. We have received quality, environmental and working environment certification.

Strålsäkerhetsmyndigheten
Swedish Radiation Safety Authority

SE-171 16 Stockholm
Solna strandväg 96

Tel: +46 8 799 40 00
Fax: +46 8 799 40 10

E-mail: registrator@ssm.se
Web: stralsakerhetsmyndigheten.se